

# High-Efficiency All-Solution-Processed Light-Emitting Diodes Based on Anisotropic Colloidal Heterostructures with Polar Polymer Injecting Layers

Andrea Castelli,<sup>†</sup> Francesco Meinardi,<sup>†</sup> Mariacecilia Pasini,<sup>‡</sup> Francesco Galeotti,<sup>‡</sup> Valerio Pinchetti,<sup>†</sup> Monica Lorenzon,<sup>†</sup> Liberato Manna,<sup>§</sup> Iwan Moreels,<sup>§</sup> Umberto Giovanella,<sup>\*,‡</sup> and Sergio Brovelli<sup>\*,†</sup>

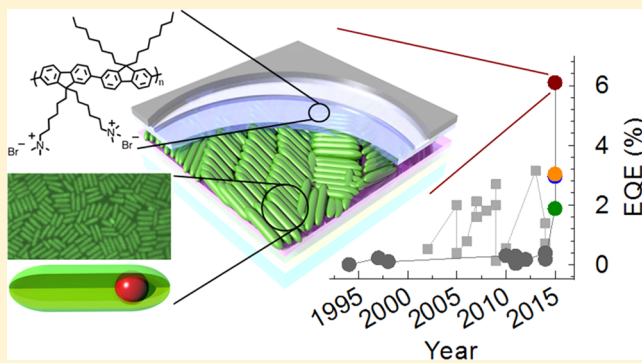
<sup>†</sup>Dipartimento di Scienza dei Materiali, Università degli Studi di Milano-Bicocca, via Cozzi 55, I-20125 Milano, Italy

<sup>‡</sup>Istituto per lo Studio delle Macromolecole, Consiglio Nazionale delle Ricerche (ISMac-CNR), Via Bassini, 15, 20133 Milano, Italy

<sup>§</sup>Istituto Italiano di Tecnologia, via Morego 30, IT-16163 Genova, Italy

## Supporting Information

**ABSTRACT:** Colloidal quantum dots (QDs) are emerging as true candidates for light-emitting diodes with ultrasaturated colors. Here, we combine CdSe/CdS dot-in-rod heterostructures and polar/polyelectrolytic conjugated polymers to demonstrate the first example of fully solution-based quantum dot light-emitting diodes (QD-LEDs) incorporating all-organic injection/transport layers with high brightness, very limited roll-off and external quantum efficiency as high as 6.1%, which is 20 times higher than the record QD-LEDs with all-solution-processed organic interlayers and exceeds by over 200% QD-LEDs embedding vacuum-deposited organic molecules.



**KEYWORDS:** Nanocrystal quantum dot, nanorods, polar polymer, solution processing, light-emitting diode, electron injecting layer

Originally descending from organic LEDs (OLEDs),<sup>1,2</sup> the quantum dot (QD)-LED design has undergone continuous evolution since the first demonstration in 1994,<sup>3</sup> exploring various charge injection/transport materials for lowering the turn-on voltage, optimizing the electron–hole balance in the emissive layer and increasing the maximum sustainable current density.<sup>4–8</sup> Concomitantly, different types of QD structures were investigated as LED emitters so as to obtain highly efficient and bright electroluminescence (EL) spanning from the UV to the near IR spectral regions.<sup>9–12</sup> The initial attempts employed a QD–polymer bilayer or binary mixture sandwiched between two electrodes<sup>13–15</sup> that, however, exhibited fairly low brightness and external quantum efficiency (EQE = 0.001–0.01%) due to degradation of the organic components at relatively low current densities, inefficient exciton formation in the QD active layer, as well as unoptimized QDs emission yields. Pioneering devices further exhibited parasitic emissions from the conjugated organic components that limited their color purity. Significant improvements were successively obtained by using thermally evaporated charge transport layers (CTLs) of small conjugated molecules that better allowed balancing the charge injection in the QDs and thereby reaching EQEs  $\geq 2.5\%$  with peak brightness of several hundreds of  $\text{cd}/\text{m}^2$  (refs 3 and 16–18). These improvements came, however, at the expense of the fabrication versatility that could no longer be conducted exclusively via solution-based processes. With the emergence of

the hybrid LED architecture, comprising both organic and inorganic CTLs, typically a ZnO nanoparticles electron transport layer (ETL) and a hole transport layer (HTL) of small organic molecules, the all-organic strategy was rapidly abandoned in favor of a disrupting design that markedly accelerated the evolution of QD-LED performances.<sup>7,11,19</sup> Using the hybrid approach, double digit EQEs were recently achieved<sup>20</sup> also with QD-LEDs fabricated via solution based methods,<sup>21</sup> which further narrowed the performance gap with the more established vacuum-deposited OLEDs.<sup>22,23</sup>

The wet processability is of key relevance for widespread application of QD-LEDs as it allows us to fully exploit the advantages of colloidal emitters for the realization of large area, flexible displays using cost-effective industrial scale-production techniques, such as roll-to-roll or inkjet printing.<sup>24–27</sup> These fabrication routes are being successfully employed in the organic electronics and photovoltaics industries, but the transfer of such protocols to QD-LEDs is proving to be difficult due to very limited options regarding orthogonal solvents for high mobility semiconducting polymers and QDs, which are both typically soluble in similar organic solvents. As a result, solution deposition of organic CTLs on a QD under-

**Received:** May 11, 2015

**Revised:** July 17, 2015

**Published:** July 22, 2015



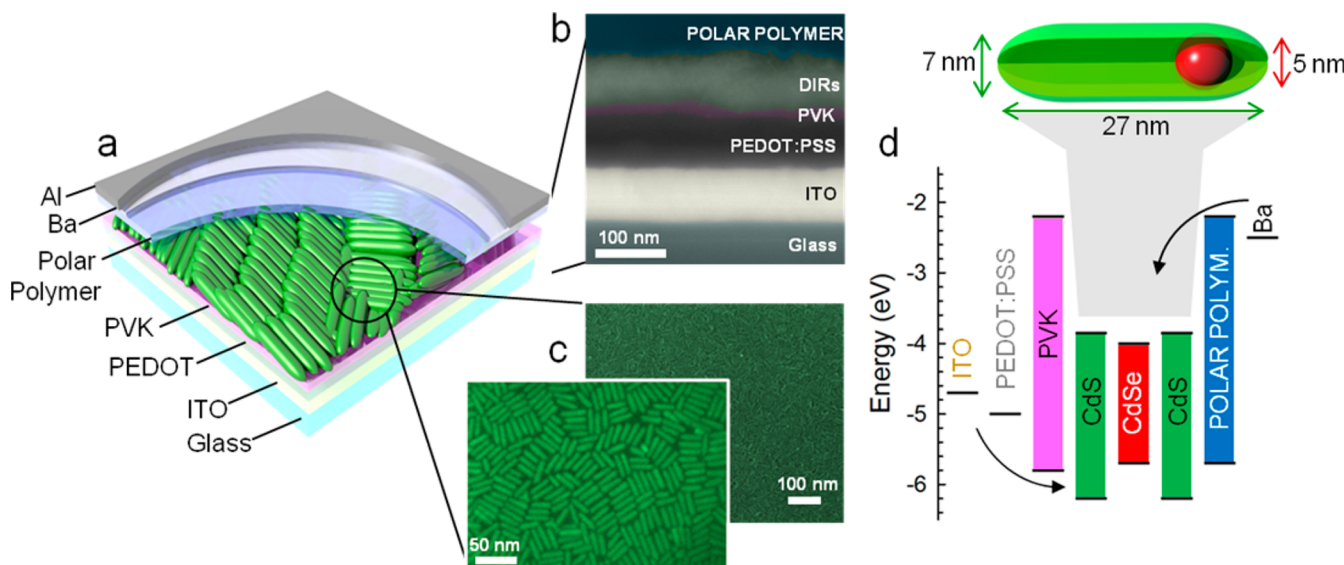


**Figure 1.** (a) Device structure of a multilayer QD-LED: ITO/PEDOT:PSS/PVK/QDs/polar-polymer-ETL/Ba/Al. (b) Cross-sectional scanning electron microscopy image of a representative DiR-LED showing the multiple layers of material with distinct contrast. The different layers are highlighted in false colors for clarity. (c) Scanning electron micrographs of the active layer of CdSe/CdS DiR-QDs prior deposition of the overlayers, showing uniform coverage (scale bar 100 nm) and the local alignment of the elongated DiR heterostructures along the *c*-axis (scale bar 50 nm). (d) Flat-band energy level diagram of the device (with respect to the vacuum level) and schematic representation of a CdSe/CdS DiR QD.

layer typically leads to its partial or complete dissolution with detrimental effects on the film homogeneity and LED performances. On the other hand, the chemical versatility of organic semiconductors could provide additional degrees of freedom for the realization of solution processable CTLs specifically functionalized so as to match the electronic properties of QDs emitting from the UV to the IR, thereby further improving the light emission performances of QD-LEDs and possibly realize efficient light-emitting structures working in spectral regions that are otherwise difficult to access. It is therefore of great technological relevance to develop strategies to compatibilize the processing protocols of semiconducting polymers and QDs for producing highly efficient and bright polymer-based QD-LEDs via industrially advantageous solution-based methods.

One important class of semiconducting polymers with growing applicative potential as solution processable charge transport materials in both organic photovoltaics and OLEDs are polar or electrolytic polymers consisting of a conjugated backbone functionalized with polar or ionic side chains that render the whole system soluble in polar environments, such as ethanol, methanol, and even water.<sup>28–32</sup> In addition to enabling processability of organic CTLs in nonsolvents for high mobility organic-soluble conjugated polymers and QDs commonly employed in multilayer LED structures, during device operation the polar functionalities align with the electric field, leading to strong polarization of the ETL/metal interface.<sup>29,31,33</sup> In OLEDs comprising of high work function metal electrodes, such as Al, the space charge region due to the aligned molecular dipoles narrows the injection barrier dramatically, allowing for electron tunneling from the cathode into the active layer, thereby reducing the turn-on voltage and increasing the EQE.<sup>29,31</sup> The effect is further enhanced in the case of electrolytic polymers charge-balanced by mobile counterions, which benefit from additional narrowing of the interfacial potential barrier for electron injection due to ion migration during device operation.<sup>32,34</sup> Therefore, as we demonstrate

below, polar/electrolytic polymers are promising materials for solution processed QD-LEDs with all-organic interlayers with charge injection and transport properties tunable by smart polymer design.

In this work, we report the first example of highly efficient and bright QD-LEDs incorporating organic CTLs fabricated exclusively via solution-based processes. Specifically, our architecture employs alcohol-soluble polyfluorene derivatives with polar/ionic functionalities as ETL in combination with polyvinyl-carbazole (PVK) as hole transport material. As emissive materials, we use so-called “dot-in-rods” (DiRs) heterostructures comprising a CdSe core incorporated in a long CdS rod. Anisotropic structures have been widely explored as emitters in lasers,<sup>35,36</sup> light down-converters,<sup>37,38</sup> and two-photon absorbers,<sup>39</sup> but their application to QD-LEDs is still marginal with respect to the traditional spherical QDs.<sup>40</sup> Nevertheless, CdSe/CdS/ZnSe nanorods have been recently shown to boost both the efficiency and brightness of QD-LEDs with respect to spherical QDs, possibly due to favorable band offset and enhanced light outcoupling,<sup>41</sup> thus making elongated structures promising candidates for high efficiency QD-LEDs. Using deep-red-emitting (650 nm) CdSe/CdS DiRs together with a polyelectrolytic ETL with mobile Br<sup>−</sup> counteranions, we obtain all-solution-based QD-LEDs with low turn-on voltage ( $V_{ON} \sim 3$  V), high brightness (1200 cd/m<sup>2</sup>), and EQE of 6.1%, which is over 1 order of magnitude higher than literature record QD-LEDs with all-solution-processed organic CTLs<sup>42–44</sup> and exceeds by ~200% the highest EQE of QD-LEDs embedding vacuum evaporated organic interlayers.<sup>45–48</sup> Importantly, QD-LEDs incorporating polyelectrolytic ETL show no roll-off of the EQE at high current densities, which further emphasizes the great applicative potential of the proposed strategy.

A schematic of the device structure and cross-sectional scanning electron microscopy (SEM) image of the QD-LEDs and corresponding flat-band energy diagram with respect to the vacuum level are shown in Figure 1a–d. The device consists of a patterned indium tin oxide (ITO) coated glass substrate with

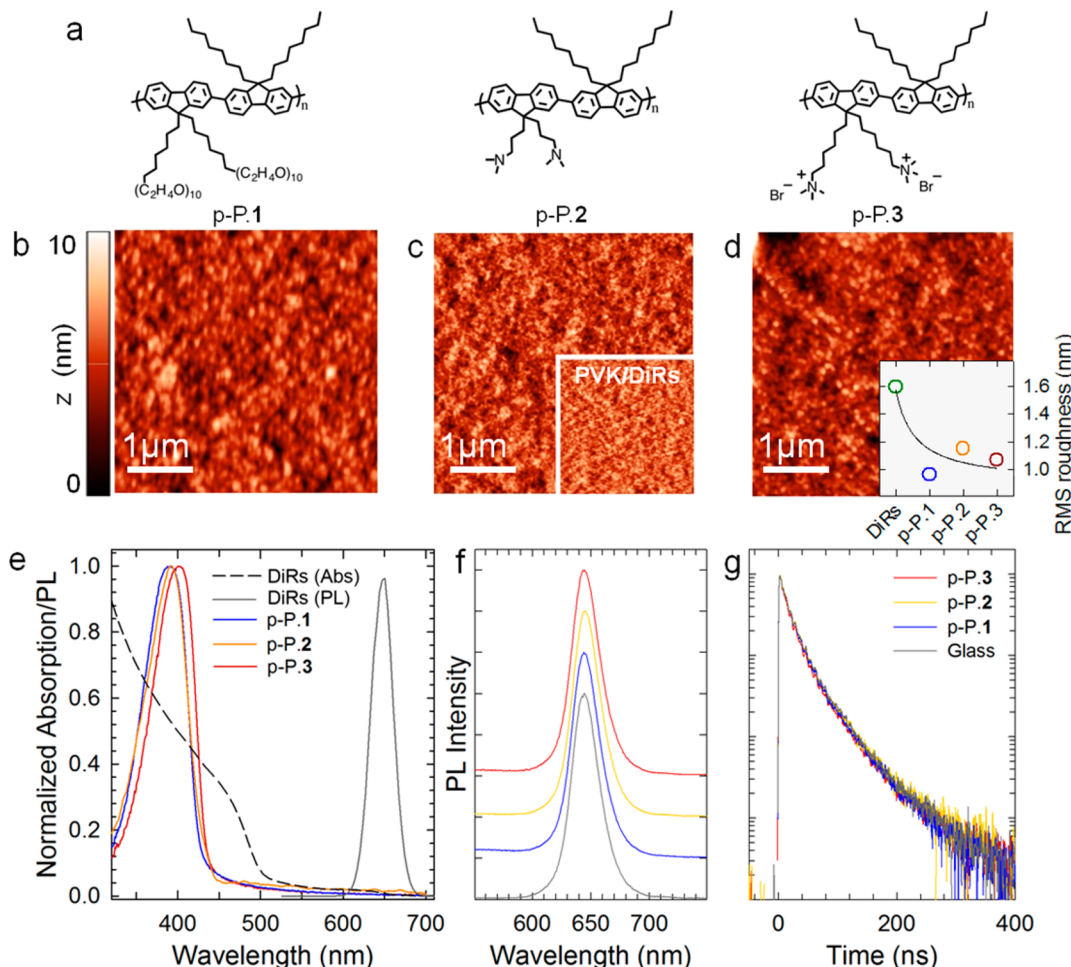


**Figure 2.** (a) Chemical structures of the alcohol-soluble polyfluorene derivatives used as ETL in all-solution processed QD-LEDs. Namely, poly[(2,7-(9,9'-dioctyl)fluorene)-*alt*-(2,7-(9,9'-bis(5"-poly(ethylene oxide)) pentyl)fluorene)] (p-P.1) and poly[(9,9'-bis(3"-(*N,N*-dimethylamino)propyl)-2,7-fluorene)-*alt*-2,7-(9,9-dioctylfluorene)] (p-P.2) are functionalized with polar side chains, while poly[(2,7-(9,9'-dioctyl)fluorene)-*alt*-(2,7-(9,9'-bis(5"-trimethylammonium bromide)pentyl)fluorene)] (p-P.3) has ionic functionalities charge-balanced by Br<sup>-</sup> counterions. AFM images ( $5 \times 5 \mu\text{m}^2$ ) obtained in tapping mode on solid films ( $\sim 30 \text{ nm}$  thickness) of (b) p-P.1, (c) p-P.2, and (d) p-P.3 spin-cast from methanol solutions on an under-layer of CdSe/CdS DiRs (dot diameter = 5 nm; rod thickness = 7 nm, rod length = 24 nm) on PVK. The AFM image of the DiR underlayer ( $2.5 \times 2.5 \mu\text{m}^2$ ) is shown in the inset of panel c. Inset of panel d is the root-mean-squared roughness values calculated from the AFM images. (e) Optical absorption of solid films of the three polymers on glass. The optical absorption and photoluminescence (PL) spectra of a diluted toluene solution of the CdSe/CdS DiRs are shown as a dashed black line and solid gray line, respectively. (f) PL spectra of submonolayer films of the same DiRs as in panel e deposited on the polar polymers, compared to the PL spectrum of the same DiRs on a glass substrate. (g) Respective PL decay curves. All PL measurements are performed using pulsed 3.1 eV excitation with power density of  $40 \text{ nJ/cm}^2$ . All measurements are carried out at room temperature. The same color scheme applies to the whole figure.

a 70 nm poly(3,4-ethylenedioxythiophene) polystyrenesulfonate (PEDOT:PSS) hole-injecting layer and a 15 nm PVK HTL that further serves to constrain inside the DiR layer electrons injected in the device from a polar-polymer ETL ( $\sim 50 \text{ nm}$ ) and an Al-capped Ba cathode (4 nm Ba; 100 nm Al). The emitting layer is a  $\sim 65 \text{ nm}$  thick film of CdSe/CdS DiRs consisting of a small CdSe core (diameter = 5.1 nm) overcoated with a 6.8 nm thick and 26.8 nm long CdS rod (see schematic in the top panel in Figure 1d and the transmission electron micrograph in Supporting Information Figure S1). These elongated heterostructures combine the advantages of high emission yield,<sup>49,50</sup> suppressed Auger recombination<sup>51,52</sup> and stability<sup>53</sup> of spherical core/shell heterostructures with the ability of nanorods to assemble into ordered anisotropic solids, which has recently been exploited to realize polarized QD-LEDs.<sup>40,54</sup> In agreement with previous observations,<sup>40,41</sup> the scanning electron micrograph of a

representative DiR film on ITO/PEDOT:PSS/PVK, before further deposition of the ETL and the metal cathode, shows a mosaic of ordered domains of DiRs aligned along their *c*-axis and further highlights the excellent layer homogeneity achievable by spin coating deposition (Figure 1c).

In order to demonstrate the potential and flexibility of polar polymers for the realization of efficient solution-processed QD-LEDs, we synthesized a pool of three polyfluorene derivatives (hereafter indicated as polar polymer p-P.1 to p-P.3 for brevity) with identical  $\pi$ -conjugated backbone and different polar/electrolytic functionalities (Figure 2a). Specifically, p-P.1 (poly[(2,7-(9,9'-dioctyl)fluorene)-*alt*-(2,7-(9,9'-bis(5"-poly(ethylene oxide)) pentyl)fluorene)]) (ref 55) and p-P.2 (poly[(9,9'-bis(3"-(*N,N*-dimethylamino)propyl)-2,7-fluorene)-*alt*-2,7-(9,9-dioctylfluorene)]) owe their polarity to the presence of heteroatoms, respectively, oxygen on the polyethylene oxide and nitrogen on the dimethylamino side chains,

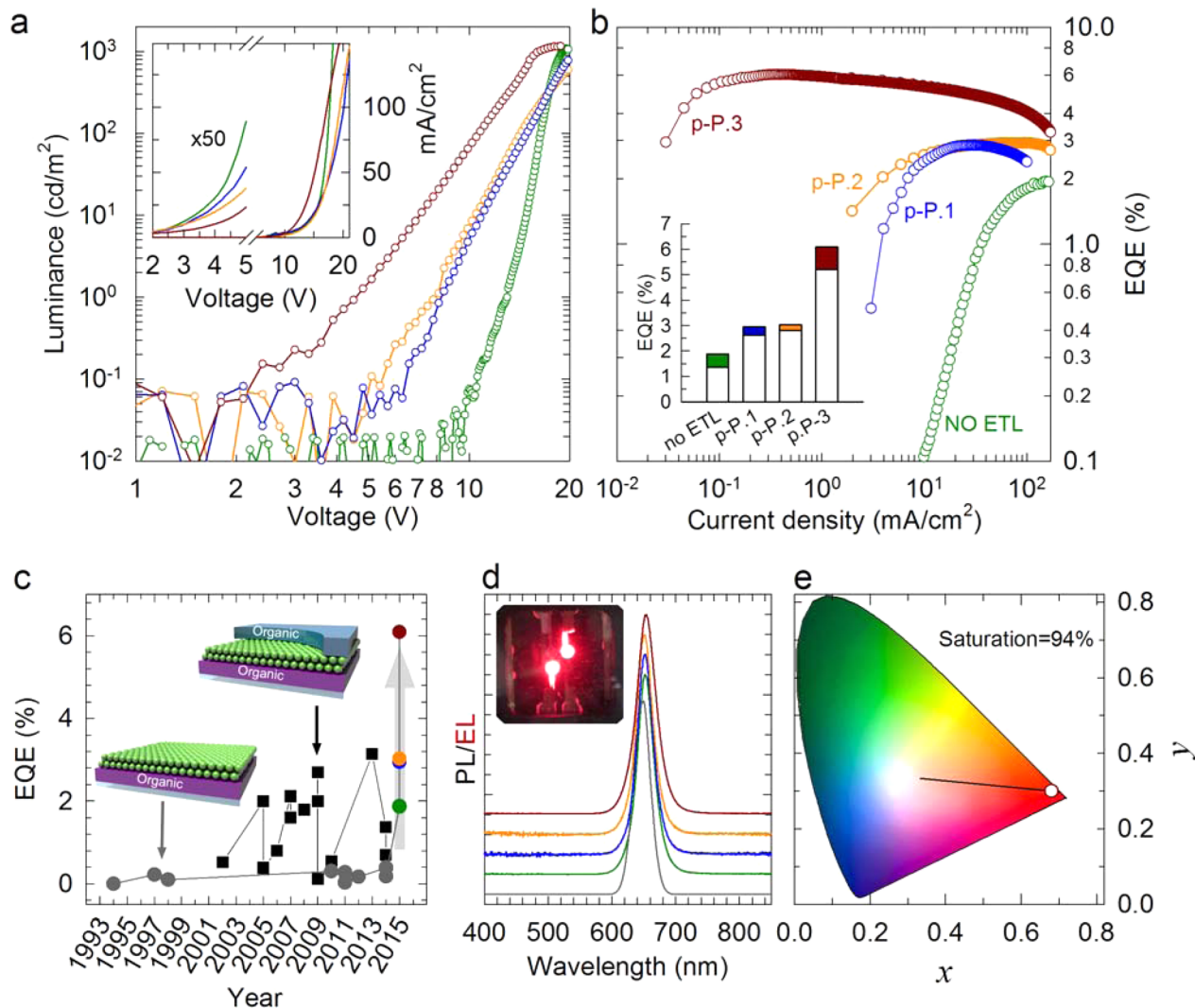


**Figure 3.** (a) Luminance–voltage ( $L$ – $V$ ) and current-density–voltage ( $J$ – $V$ , inset) responses of fully solution processed QD-LEDs embedding CdSe/CdS DiRs and different polar/electrolytic polymeric ETL (device structure ITO/PEDOT:PSS/PVK/DiRs/polar-polymer ETL/Ba/Al). The  $J$ – $V$ – $L$  response for a control device without the ETL is reported for direct comparison. The low-voltage portion (2–5 V) of the  $J$ – $V$  curve is scaled by a factor of 50 to emphasize the electric behavior close to turn-on for the LEDs with polymer ETLs. (b) Corresponding EQE as a function of the current density. Inset: EQE for a set of 10 devices. The maximum absolute value is indicated by the height of the columns while the statistics over the device set is indicated by the width of the colored area. (c) Chronological evolution of the EQE of QD-LEDs embedding organic CTLs since the first demonstration in 1994. LEDs consisting of QDs embedded in or deposited on top of polymeric CTLs are shown as gray dots (refs 3, 13–15, 42–44, and 68). The black squares refer instead to QD-LEDs with thermally evaporated CTLs of small organic molecules (refs 10, 17, 18, 45–47, and 69–74). The colored dots indicate the EQE values obtained in this work. (d) Electroluminescence spectra of the devices embedding the different polar/ionic polymer ETLs compared to the PL spectrum of the DiRs on glass (gray line). A photograph of a working LED with p-P.3 interlayer is reported in the inset showing uniform bright emission over the whole device area (driving bias 5.5 V). (e) Corresponding chromaticity coordinates in the CIE chromaticity diagram, highlighting the vicinity of the color coordinates to the spectral locus. The same color scheme applies to the whole figure.

while p-P.3 (poly[(2,7-(9,9'-dioctyl)fluorene)-*alt*-(2,7-(9,9'-bis-(5"-trimethylammonium bromide)pentyl)fluorene)]) is a poly-electrolyte functionalized with trimethylammonium ionic groups with Br<sup>-</sup> counterions. All systems were further substituted with octyl side-chains to hinder intermolecular aggregation and crystallization of the film.<sup>56</sup> The functionalized polymers show good film forming properties by spin-coating from methanol solution that, being a nonsolvent for the DiRs with hexylphosphonic and octadecylphosphonic acid ligands, successfully avoids compromising the integrity of the active layer while depositing the ETL. Accordingly, we observe no damage or degradation of the under-layers upon spin-casting the overlayers (see Figure 1b). Interestingly, atomic force

microscopy (AFM) images of polymer films spin coated on a PVK/DiRs bilayer reveal a measurable decrease of the film roughness (Figure 2b–d). In the inset of Figure 2d, we report the root-mean-square roughness calculated from  $5 \times 5 \mu\text{m}^2$  images, obtained in tapping mode on spin-cast polymer films (~30 nm thickness).

Importantly, the functionalization with the polar side chains does not interfere with the conjugated  $\pi$ -orbitals of the polyfluorene backbone and thus leads to no modification in the position of the HOMO and LUMO levels.<sup>57,58</sup> As a result, all polymers exhibit a comparable absorption spectrum typical of polyfluorenes<sup>28</sup> with a low energy absorption band at approximately 395 nm,<sup>56,58</sup> as shown in Figure 2e together

with the optical properties of the CdSe/CdS DiRs. In these heterostructures, similar to zero- and bidimensional core/shell CdSe/CdS systems,<sup>59</sup> the large (400 meV) energy offset between the CdSe and CdS valence bands along with the essential alignment of the conduction band energy (Figure 1d) leads to the formation of a quasi-type II heterojunction<sup>39</sup> where the hole wave function is localized inside the CdSe dot while the electron wave function spreads over the rod region within the attractive Coulomb potential of the hole. Because of the extremely rapid transfer of holes from the rod to the dot (<1 ps; ref 51), emission from these systems is typically dominated by recombination of CdSe excitons, while light absorption is due to the much larger CdS rod that accounts for the majority of the particle volume (>93% in the current case). As a result, the absorption spectrum shows a steep edge at approximately 475 nm due to absorption transition between band-edge states of the CdS rod, while the Stokes-shifted photoluminescence (PL) peaked at 650 nm arises from the radiative recombination of band-edge excitons in the CdSe dot (Figure 2e). The characteristic quasi type II confinement regime provides a further advantage to CdSe/CdS heterostructures over conventional core-only QDs, that is, the effective protection of the electron–hole pair from detrimental charge trapping processes involving surface sites or environmental agents.<sup>60</sup> As a result, CdSe/CdS systems with thick shells have been successively applied to various photonic devices including LEDs,<sup>61</sup> lasers<sup>36,62</sup> and luminescent solar concentrators based on QD-polymer composites fabricated via radical polymerization routes.<sup>37,63</sup>

The preservation of the optical properties of the emitters upon incorporation in the device is of key relevance also to assess the suitability of polar polymers as ETL materials for QD-LEDs. Specifically, in order to be successfully employed for the fabrication of efficient LEDs, it is strictly necessary that they do not quench the DiR emission by activating nonradiative relaxation channels, such as rapid hole transfer to the electron rich polar side chains and to the counteranions, or electron transfer to the cationic functionalities that could in principle act as highly efficient electron harvesters, leaving the QD positively charged.<sup>21</sup> The effects of positive or negative charging of QD by electron transfer from or to polymer interlayers or ZnO nanoparticles in both direct and inverted structure LEDs have been recently investigated by several groups showing detrimental effects on the device efficiency and stability.<sup>21,64–67</sup>

In order to test charging/quenching effects by our polymer materials, we measured the PL efficiency and dynamics of CdSe/CdS DiRs on glass and deposited on top of ~60 nm films of each polar polymer. The data reported in Figure 2f,g show remarkable invariance of both the PL spectrum and efficiency measured with an integrating sphere that in all cases is  $\Phi_{PL} = 54 \pm 5\%$ . Accordingly, the PL decay dynamics is identical for all substrates, which further confirms the compatibility of the polar polymers with the optical properties of the DiRs and, as we show below, the all-solution-based process used to fabricate the QD-LEDs.

Figure 3 reports the current density–voltage–luminance ( $J-V-L$ ) response of a set of QD-LEDs embedding the different polar polymer ETL (namely, ITO/PEDOT:PSS/PVK/DiRs/p-P ETL/Ba/Al) in comparison to a reference device of identical structure except without the ETL. For the fabrication of the devices, we used water, chlorobenzene, toluene, and methanol as the solvents for PEDOT:PSS, PVK, CdSe/CdS DiRs, and the polar polymer ETLs, respectively. All devices were

preconditioned in order to polarize the ETL/cathode interface as commonly performed for LECs and OLEDs with ionic/polar interlayers (Supporting Information Figure S2<sup>31</sup>). After conditioning, the devices are stable for many successive sweeps and for over twenty hours under continuous operation (see Supporting Information Figures S3 and S4). The turn-on voltage ( $V_{ON}$ , measured as the voltage at which the luminance is 0.1 cd/m<sup>2</sup>) of LEDs embedding polar ETLs is markedly lower with respect to the control device (~6.4 V for p-P.1 and ~5.4 V for p-P.2 vs ~8 V for the control LED). The effect is even stronger for the LEDs incorporating p-P.3 that turn on at  $V_{ON} \sim 2.7$  V, which is just above the band gap energy of the CdS rod (~2.61 eV, see absorption onset energy in Figure 1e). Concomitantly to the drop of  $V_{ON}$ , the luminance increases, leading to the progressive growth of the maximum EQE from 1.8% for the reference device to 6.1% for the QD-LED incorporating p-P.3, as shown in Figure 3b that further highlights the shift of the EQE curves toward lower current densities, in agreement with the gradually lower  $V_{ON}$ . Importantly, the LED with p-P.3 ETL shows very weak roll-off of the EQE (Figure 3b), which is maintained >4% for current densities as high as  $J = 120$  mA/cm<sup>2</sup> and brightness in the range 100–1200 cd/m<sup>2</sup>, corresponding to the luminance requirements for display applications. The achieved 6.1% efficiency is the highest value ever reported for QD-LEDs incorporating all-organic CTLs produced both via solution based methods and thermal evaporation, as summarized in Figure 3c where we report the chronological evolution of the EQE of QD-LEDs with all-organic layers since the first demonstration in 1994.<sup>3</sup> The plot further highlights that our DiR-LEDs without polymer ETL already largely outperform previous devices with similar structure embedding spherical QDs (gray circles, EQE  $\leq 0.5\%$ ) and nearly match the efficiency of record QD-LEDs with vacuum evaporated CTLs. In this regard, it is important to notice that our DiRs were not optimized in terms of emission efficiency ( $\Phi_{PL} = 54\%$ ), while the spherical QDs used in literature studies typically exhibited  $\Phi_{PL} > 90\%$ . This suggests a critical role of the DiR emissive layer in the device performances in combination with improvements afforded by the polar polymer ETLs. To test this effect, we fabricated and tested QD-LEDs embedding spherical CdSe/CdS core/shell QDs (core diameter = 4 nm, shell thickness = 2 nm with  $\Phi_{PL} \sim 85\%$ ) and the different polymer ETLs. The data, reported in Supporting Information Figure S5, confirm the superior performance of anisotropic structures, revealing approximately 10× lower EQEs with respect to the DiR-based LEDs, which is in agreement with recent observations.<sup>41</sup> Nevertheless, the insertion of polymer ETLs in LEDs featuring spherical QDs yields EQEs as large as 1%, which is above state of the art for QD-LEDs based on solution processed organic interlayers.<sup>42–44</sup> Because enhanced EQEs are obtained with DiRs featuring lower  $\Phi_{PL}$  with respect to the spherical QD counterparts, the results suggest that the anisotropic shape of the emitters might boost the EQE by improving the light outcoupling, rather than by enhancing the internal quantum efficiency. Recently, variable angle spectroscopic ellipsometry measurements by Nam et al.<sup>41</sup> indicated optical anisotropy in heterostructured nanorods films resulting from the emissive dipoles being mostly parallel to the device surface and leading to suppression of optical losses due to directional emission toward the device edges.<sup>75–77</sup> However, the angular profile of the EL intensity for DiR- and QD-based LEDs reported in Supporting Information Figure S6 shows that

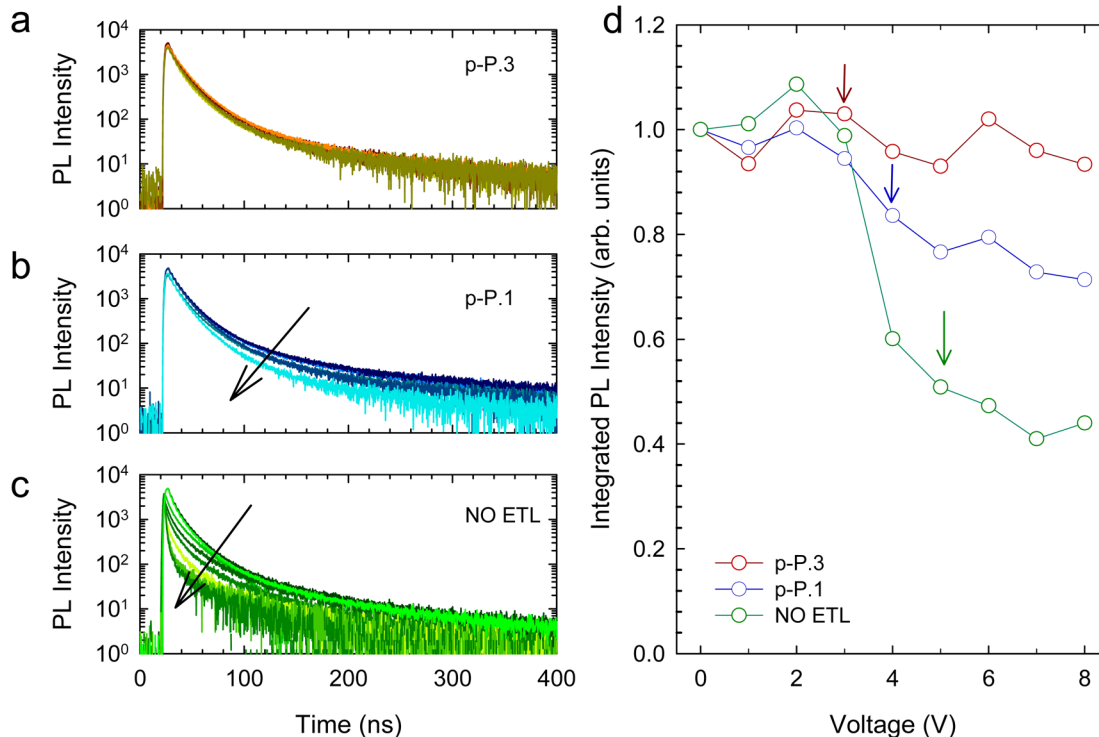


**Figure 4.** Photoluminescence decay curves of CdSe/CdS DiRs incorporated in LEDs of identical structure (ITO/PEDOT:PSS/PVK/DiRs/polar-polymer ETL/Ba/Al) but with different ETL collected during device operation (black arrows indicate increasing driving voltage from 0 to 8 V). The QD-LED in (a) features an ETL of p-P.3, the device in (b) incorporates p-P.1, while (c) shows the data for the control LED with no ETL. All measurements were conducted using pulsed 3.1 eV. The time integrated PL intensity versus voltage for the three samples is shown in (d). The colored arrows indicate the turn on voltage of each device.

both devices exhibit Lambertian emission distribution, which might suggest that such effect is not dominant in our DiR-LEDs possibly due to random orientation of the DiRs in the 6–7 monolayers thick active layer.

The EL spectra of the whole set of QD-LEDs are shown in Figure 3d, together with a photograph of a working LED, showing uniform illumination across the whole electrode ( $5.4 \text{ mm}^2$ ). For all devices, the symmetric and narrow (full width at half-maximum = 30 nm) spectrum is peaked at  $\sim 650 \text{ nm}$ , corresponding to the Commission Internationale de l'Eclairage (CIE) color coordinates of ( $x = 0.72$ ,  $y = 0.29$ ), which represent color-saturated (saturation 94%) deep-red light ideal for RGB display applications (Figure 3e). We highlight that the obtained peak brightness ( $>1000 \text{ cd/m}^2$ ) is particularly remarkable if one considers that the EL lies in the very low sensitivity tail of the human eye response. Importantly, for all polymers the EL spectrum shows no spurious emission from the organic components, which indicates that in our devices' excitons are effectively formed inside the DiRs active layer.

We now discuss the role of the polar polymer ETLs in the achieved device performance. Although the exact mechanism by which polar polymer ETLs boost the efficiency of both OLEDs and PV cells is still disputed,<sup>29,31</sup> analysis of the spectroscopic and electro-optical data suggests that in our case the observed improvements results from better electron–hole balance in the DiR layer afforded by the introduction of a thin electron injection barrier that mitigates the electron inflow in the device. Looking at the energy diagram in Figure 1d, we note that the Fermi level of the Ba cathode is well above the conduction band of both CdSe and CdS, which facilitates electron injection in the DiRs without the need to overcome any potential barrier

except that imposed by the dielectric passivation of the particle surfaces. At the opposite end of the diode, holes encounter a steplike potential barrier with a last moderate offset ( $\sim 0.4 \text{ eV}$  in flat band conditions) due to the lower energy of the CdS valence band with respect to the HOMO level of PVK. Therefore, in control devices holes are minority carriers while excess electrons accumulate at the interface between the DiRs and the PVK blocking layer. As a result, the relatively lower performance of the control device with respect to LEDs with polar polymer ETLs is ascribed to partially impeded hole injection leading to insufficient hole concentration in the emissive layer, as commonly observed for unbalanced LEDs based on CdSe/CdS QDs.<sup>61</sup> This further implies that the beneficial role of the polar polymers in our QD-LEDs is not directly related to their ability to boost electron injection by creating interfacial dipoles, as instead observed in OLEDs with large work function metal electrodes where holes are the majority carriers and electron injection is the bottleneck process<sup>31</sup> but is rather associated with the introduction of a  $\sim 0.3 \text{ eV}$  energy barrier at the cathode. This positive energy offset, nearly matching the hole injection barrier at the PVK/DiR interface, contrasts the injection of electrons and thereby boosts the EQE by balancing the charge population in the emissive layer. Accordingly, LEDs incorporating polymer ETL show lower current at driving bias close to  $V_{\text{ON}}$  with respect to the control device in which electric transport is sustained by electrons easily injected from the Ba electrode (Figure 3a,b). Excessive electron concentration in QD-LEDs has been demonstrated to lead to negative charging of the QDs<sup>21,45,65</sup> with consequent dimming of the emission due to Auger recombination.<sup>64</sup> This effect can be mitigated by using

interlayers capable of reducing the electron inflow in the device, as recently shown for hybrid structure QD-LEDs with a thin dielectric layer placed between the QDs and the ZnO nanoparticles ETL.<sup>21</sup> This scenario describes well the behavior of our QD-LEDs in which the polar polymer ETLs introduce a moderate injection barrier at the cathode that controls electron injection, lowering the current and concomitantly increasing the brightness.

In order to provide direct evidence of the photophysical implication of improved charge balance in QD-LEDs with polar/polyelectrolytic ETL, we compare in Figure 4 time-resolved PL measurements performed under electric drive for a control device and for LEDs embedding p-P.1 and p-P.3. Remarkably, the PL dynamics of DiRs embedded in LEDs with polyelectrolytic ETL are completely unvaried even at driving voltages well above  $V_{ON}$ , that is, when charges are directly injected in the DiR quantized states, thus confirming that the DiRs remain in their uncharged emissive state. On the other hand, in the absence of ETL the PL dynamics progressively accelerates with increasing driving bias and the emission intensity drops, most likely as a result of charging and consequent nonradiative Auger recombination. Accordingly, the PL intensity for LEDs with p-P.3 is completely independent of the applied voltage, while for the control device it undergoes a ~60% drop. Importantly, we observe that in all investigated LEDs, with or without ETL, the PL dynamics at  $V = 0$  V is essentially identical to that of DiR deposited on glass (Figure 2g), which indicates that the emission efficiency is unaffected by the top metal electrode, which is in agreement with the protective effect of the CdS shell on core excitons. This further confirms that the higher efficiency obtained through the insertion of the polymer ETLs is due to improved device operation and not to suppressed quenching by the metal cathode.

Finally, it is worth noting that in contrast to dielectric interlayers, polar or electrolytic polymers introduce a dynamic potential barrier at the cathode, whose width can be finely tuned by the rearrangement of the polar side chains and by the progressive formation of a charged region close to the ETL/metal boundary. This implies that the modulation of the electron inflow is not determined by the height of the potential barrier in flat band conditions but rather by the ability of the interface to polarize and thereby to promote electron tunnelling. This effect is clearly observed during conditioning voltage sweeps that lead to progressively lower  $V_{ON}$  and higher EQEs (Supporting Information Figure S2). In this regard, we further note a marked difference between the dynamic electrical behavior of LEDs with polar (p-P.1) or ionic (p-P.3) ETL. Specifically, complex impedance spectroscopy measurements reported in Supporting Information Figure S7 show that upon conditioning (up to 10 V), LEDs with polar ETL undergo rapid and intense increase of electron injection, leading to over 50% drop of the device capacitance with respect to unbiased conditions due to facilitated charge tunnelling through the barrier. In contrast, LEDs with electrolytic ETL show only a weak reduction of the electron injection resistance and over 4-fold increase of the capacitance, as a result of progressive accumulation of the  $\text{Br}^-$  counteranions at the ETL/DiR interface. The two devices further show significant difference between the time evolution of their capacitance: LEDs with polar ETL rapidly recover the initial value, while the recovery time is much longer for devices with ionic ETL due to slow ion redistribution across the polymer film. This is in agreement

with the significantly slower growth of the electric current under constant driving bias in LEDs with ionic with respect to polar ETL (Supporting Information Figure S8). The whole body of electric transport and dielectric response data suggests that the better EL performances obtained using ionic p-P.3 might be due to partial retention of electron injection barrier, which better controls the charge balance inside the device (also in agreement with the lower current in Figure 3a). This further indicates that the electric response of polar/electrolytic polymers can be fine-tuned by suitable choice of both the side-chains and the counterions,<sup>30,31,33</sup> providing a strategy for optimizing charge injection and transport via rational polymer design.

In conclusion, we demonstrated the first example of high efficiency QD-LEDs featuring all-solution-processed organic charge transport layers that outperform all previously reported QD-LEDs based on all-organic interlayers. Without using an advanced factory facility, we obtained record EQE = 6.1% and very limited efficiency roll-off, suggesting enormous potential improvements by using optimized industrial fabrication equipment. Further large improvements could also be achieved by optimizing the QD active layer in terms of emission quantum yield. We highlight that the reported devices were tested without encapsulation. The impressive performances are ascribed to the combined use of anisotropic elongated heterostructures and polar polymer electron transport layers that control electron injection and balance the charge population inside the device. Although detailed understanding of the physical mechanisms underpinning the device operation will require further dedicated investigations, our results clearly demonstrate an effective strategy for compatibilizing the cost-effective solution-based protocols used by the organic electronic industry and colloidal semiconductor quantum structures for the realization of high efficiency, high color purity and bright QD-LEDs on large-area, flexible substrates for display, and solid-state lighting applications.

**Methods.** 1. *Synthesis and Characterization of Polar and Electrolytic Polymers.* Polar polymer p-P.1: poly[(2,7-(9,9'-diethyl)fluorene)-*alt*-(2,7-(9,9'-bis(5"-poly(ethylene oxide)) pentyl)fluorene)]. A mixture of 9,9-diethylfluorene-2,7-diboronic acid bis(1,3-propanediol) ester (40 mg, 0.07 mmol), 2,7-dibromo- 9,9'-bis(5"-poly(ethylene oxide) pentyl)fluorene (100 mg, 0.7 mmol),  $\text{PdCl}_2(\text{PPh}_3)_2$  (0.5 mg, 0.0007 mmol), degassed aqueous sodium carbonate (2 M, 2 mL), and tetrahydrofuran (THF) (4 mL) was introduced in a Schlenk tube under nitrogen atmosphere. The reaction mixture was stirred for 3.5 h at 70 °C. The end groups were capped by additional 4 h reaction in excess of bromobenzene (0.15 mmol) and further 4 h in excess of phenylboronic acid pinacol ester (0.15 mmol). After cooling to room temperature and removing the aqueous phase, the mixture was stirred overnight with 3-mercaptopropyl-functionalized silica gel (Pd scavengers), filtered on PTFE membrane, and dried. The collected solid was placed in a Soxhlet apparatus, washed for one night with hexane, and then extracted with methanol to afford the product with a yield of 45%.

<sup>1</sup>H NMR ( $\text{CDCl}_3$ , 600 MHz,  $\delta$ , ppm): 7.86 (4H, d, fluorenyl group), 7.69 (8H, m, fluorenyl group), 3.67–3.40 (82H, m,  $-\text{CH}_2\text{O}-$  and  $-\text{OCH}_3$ ), 1.70 (22H, s,  $-\text{CH}_2\text{O}-$  and  $-\text{CH}_2-$ ), 1.22 (28H, s,  $-\text{CH}_2\text{O}-$  and  $-\text{CH}_2-$ ), 0.83 (20H, m,  $-\text{CH}_2\text{O}-$ ,  $-\text{CH}_3$  and  $-\text{CH}_2-$ ).

GPC (THF, polystyrene standard) analysis showed a  $M_w$  = 15 000 and PDI = 1.58.

Polar polymer p-P.2: poly[(9,9'-bis(3''-(*N,N*-dimethylamino)propyl)-2,7-fluorene)-*alt*-2,7-(9,9-diethylfluorene)]. A mixture of 2,7-dibromo-9,9'-bis(3''-(*N,N*-dimethylamino)propyl)fluorene (150 mg, 0.3 mmol), 9,9-diethylfluorene-2,7-diboronic acid bis(1,3-propanediol) ester (168 mg, 0.3 mmol), PdCl<sub>2</sub>(PPh<sub>3</sub>)<sub>2</sub> (2 mg, 0.003 mmol), degassed aqueous potassium carbonate (2 M, 6 mL), and THF (12 mL) was introduced in a Schenk tube under nitrogen atmosphere. The reaction mixture was stirred for 1 h at 70 °C. Then the end groups were capped by stirring the mixture at 70 °C for 2 h in excess of bromobenzene (0.4 mmol) and for further 2 h in excess of phenylboronic acid pinacol ester (0.4 mmol). After cooling to room temperature, the organic phase was precipitated in 200 mL of methanol to afford the product as green-yellow powder with a yield of 60%.

<sup>1</sup>H NMR (600 MHz, CDCl<sub>3</sub> + CD<sub>3</sub>OD): δ 7.74–7.57 (12H, m, fluorenyl group), 2.10–1.96 (24H, m, –CH<sub>2</sub>N, –NCH<sub>3</sub>, –CH<sub>2</sub>–), 1.04–0.92 (26H, m, –CH<sub>2</sub>–), 0.67–0.58 (12H, m, CH<sub>3</sub> and –CH<sub>2</sub>–).

GPC (THF, polystyrene standard) analysis showed a  $M_w$  = 36 000 and PDI = 3.04.

Polar polymer p-P.3: poly[(2,7-(9,9'-diethylfluorene)-*alt*(2,7-(9,9'-bis(5''-trimethylammonium bromide)pentyl)-fluorene)]]. A mixture of 2,7-dibromo-9,9'-bis(5''-bromopentyl)fluorene (100 mg, 0.16 mmol), 9,9-diethylfluorene-2,7-diboronic acid bis(1,3-propanediol) ester (899 mg, 0.16 mmol), PdCl<sub>2</sub>(PPh<sub>3</sub>)<sub>2</sub> (1 mg, 0.0015 mmol), degassed aqueous potassium carbonate (2 M, 1.5 mL), and THF (3 mL) was introduced in a Schenk tube under nitrogen atmosphere. The reaction mixture was stirred for 4 h at 70 °C. The end groups were capped by additional 4 h reaction in excess of bromobenzene (0.16 mmol) and further 4 h in excess of phenylboronic acid pinacol ester (0.16 mmol). After cooling to room temperature, the organic phase was precipitated in 150 mL of methanol to afford the neutral precursor polymer with a yield of 81%.

<sup>1</sup>H NMR (CDCl<sub>3</sub>, 600 MHz, δ, ppm): 7.83 (4H, d, fluorenyl group), 7.67 (8H, m, fluorenyl group), 3.28 (4H, t, –CH<sub>2</sub>Br), 2.10 (8H, m, –CH<sub>2</sub>–), 1.68 (4H, m, –CH<sub>2</sub>–), 1.60 (4H, m, –CH<sub>2</sub>–), 1.12 (22H, m, –CH<sub>2</sub>–), 0.76 (12H, m, CH<sub>3</sub> and –CH<sub>2</sub>–).

GPC (THF, polystyrene standard) analysis showed a  $M_w$  = 54 000 and PDI = 3.57.

The cationic polymer was obtained by trimethylamine ionization of the neutral precursor, referring to a reported procedure.<sup>78</sup> Twelve milliliters of a 1:2 v/v solution of condensed trimethylamine in THF were added dropwise to a stirring solution of the neutral precursor polymer (100 mg) in 10 mL of THF at –78 °C. The mixture was then allowed to warm up to room temperature and then stirred overnight. After the solvent was removed, the salified polymer was recovered as a white powder in quantitative yield.

<sup>1</sup>H NMR (600 MHz, CD<sub>3</sub>OD): δ 7.91–7.76 (12H, m, fluorenyl group), 3.15 (4H, m, –CH<sub>2</sub>N), 2.99 (18H, s, –NCH<sub>3</sub>), 1.65 (6H, m, –CH<sub>2</sub>–), 1.32–1.22 (8H, m, –CH<sub>2</sub>–), 1.13 (28H, m, –CH<sub>2</sub>–), 0.74 (12H, m, CH<sub>3</sub> and –CH<sub>2</sub>–).

2. *Synthesis of CdSe/CdS Dot-in-Rod QDs.* CdSe/CdS dot-in-rod QDs were prepared according to established synthesis procedures.<sup>79</sup> The core diameter (5.1 nm), as well as the rod diameter (6.8 nm) and length (26.8 nm), were determined with transmission electron microscopy.

3. *Film Characterization and Microscopy.* Atomic force microscopy investigations were performed using a NT-MDT

NTEGRA instrument in semicontact mode in ambient conditions. Scanning electron microscopy images of the QD film and device structure were collected with a JEOL JSM-7500FA high-resolution field emission scanning electron microscope at an accelerating voltage of 15 kV.

4. *Device Fabrication and Characterization.* For the fabrication of LEDs, glass substrates (25 × 25 × 1.1 mm<sup>3</sup>) coated with ITO (sheet resistance 15 Ω/sq) were mechanically cleaned with acetone and optical paper, sonicated at 45 °C in N-propanol and treated in 3 mbar O<sub>2</sub> plasma for 10 min. Immediately after the plasma treatment, a 70 nm thick PEDOT:PSS (Heraeus) film was spin coated in air over the ITO (spin coating parameters: 2000 rpm for 60") and thermally annealed at 150 °C inside N<sub>2</sub> filled glovebox for 10 min. The high-temperature annealing yields a compact hole-conducting layer. After cooling, a thin (15 nm) PVK hole-transport layer was spin-coated from a 15 mg/mL chlorobenzene solution and annealed at 150 °C for 10 min. The active QD layer (65 nm) was successively spin-coated from a 30 mg/mL toluene solution. For the deposition of the polymer ETL, p-P.1 and p-P.3 were dissolved in pure methanol (5 mg/mL). For p-P.2 (2.5 mg/mL), 10 μL/ml of acetic acid were added to methanol. The metal cathode consisting of a 4 nm Ba layer coated with 100 nm Al capping layer was finally thermally evaporated in high vacuum ( $5 \times 10^{-7}$  bar). The final device area is 5.4 mm<sup>2</sup>. A Keithley 2602 source meter was used to measure the current–voltage–luminance characteristics of the devices. The light output was measured by a calibrated silicon photodetector (Thorlabs FDS1010 photodiode, active area: 1 cm<sup>2</sup>) positioned at a fixed distance and directed toward the ITO glass side of the device. The LED brightness was determined from the fraction of light that reaches the photodetector. The EL spectra were recorded with a Spex 270 M spectrometer coupled to a charged couple device. LEDs were tested in nitrogen atmosphere without additional environmental protection. The devices were stored under ambient conditions between experiments. Stability measurements were conducted using the same setup while driving the LEDs in constant current mode.

5. *Optical Spectroscopy.* The absorption spectra were recorded using a PerkinElmer Lambda 900 spectrometer. The photoluminescence measurements were performed using a pulsed diode laser at 405 nm (Edinburg Inst. EPL 405, 40 ps pulse width) as excitation source and collecting the emitted light with a charged coupled device coupled to a spectrometer. Time-resolved photoluminescence experiments were conducted using the same excitation source and collecting with a time-correlated single photon counting unit coupled to a monochromator and a photomultiplier tube. Time-resolved measurements during device operation were performed in backscattering geometry by exciting the DiR active layers through the glass substrate directly under the metal cathode. All PL measurements were performed with power density of 40 nJ/cm<sup>2</sup>. All measurements were carried out at room temperature.

6. *Impedance Spectroscopy and Capacitance Measurements.* Impedance spectroscopy and capacitance measurements were performed in nitrogen atmosphere using a Bio Logic SP-200 Research grade Potentiostat/Galvanostat. The LEDs were tested before conditioning using oscillating voltage of ±0.1 V and after conditioning steps of 2 V for 30 s up to 10 V. After each conditioning step, the bias was brought back to 0 V before performing the impedance measurement. For

measuring the time evolution of the capacitance after conditioning, unconditioned LEDs were first biased for 5 min at 10 V and successively scanned repeatedly for 30 min.

## ■ ASSOCIATED CONTENT

### Supporting Information

The Supporting Information is available free of charge on the ACS Publications website at DOI: [10.1021/acs.nanolett.5b01849](https://doi.org/10.1021/acs.nanolett.5b01849).

Additional TEM characterization, LEDs based on spherical core/shell QDs, device lifetime and emission profile data, as well as impedance spectroscopy and capacitance characterization. ([PDF](#))

## ■ AUTHOR INFORMATION

### Corresponding Authors

\*E-mail: [sergio.brovelli@unimib.it](mailto:sergio.brovelli@unimib.it) (S.B.).

\*E-mail: [u.giovanella@ismac.cnr.it](mailto:u.giovanella@ismac.cnr.it) (U.G.).

### Present Address

(A.C.) Istituto Italiano di Tecnologia, via Morego 30, IT-16163 Genova, Italy.

### Notes

The authors declare no competing financial interest.

## ■ ACKNOWLEDGMENTS

S.B., F.M., M.P., and U.G. acknowledge support from Cariplò Foundation (2012-0844). F.M. acknowledge support from Cariplò Foundation (2010-0564). S.B. wishes to thank the European Community's Seventh Framework Programme (FP7/2007-2013) under grant agreement N. 324603 for financial support (EDONHIST). U.G., M.P., and F.G. thank the Regione Lombardia for financial support (decreto 3667/2013). M.L. acknowledges support from Fondazione Cassa di Risparmio di Tortona. F. De Donato is acknowledged for synthesizing the CdSe/CdS dot-in-rod QDs, and A. Scarpellini for valuable assistance with the SEM measurements. This work is dedicated to the loving memory of Gianluca Latini, friend and colleague.

## ■ REFERENCES

- Shirasaki, Y.; Supran, G. J.; Bawendi, M. G.; Bulovic, V. *Nat. Photonics* **2012**, 7 (1), 13–23.
- Talapin, D. V.; Steckel, J. *MRS Bull.* **2013**, 38 (09), 685–691.
- Colvin, V. L.; Schlamp, M. C.; Alivisatos, A. P. *Nature* **1994**, 370 (6488), 354–357.
- Bae, W. K.; Kwak, J.; Lim, J.; Lee, D.; Nam, M. K.; Char, K.; Lee, C.; Lee, S. *Nano Lett.* **2010**, 10 (7), 2368–2373.
- Caruge, J. M.; Halpert, J. E.; Wood, V.; Bulovic, V.; Bawendi, M. G. *Nat. Photonics* **2008**, 2 (4), 247–250.
- Cho, K. S.; Lee, E. K.; Joo, W. J.; Jang, E.; Kim, T. H.; Lee, S. J.; Kwon, S. J.; Han, J. Y.; Kim, B. K.; Choi, B. L.; Kim, J. M. *Nat. Photonics* **2009**, 3 (6), 341–345.
- Kwak, J.; Bae, W. K.; Lee, D.; Park, I.; Lim, J.; Park, M.; Cho, H.; Woo, H.; Yoon, D. Y.; Char, K.; Lee, S.; Lee, C. *Nano Lett.* **2012**, 12, 2362–2366.
- Wood, V.; Panzer, M. J.; Halpert, J. E.; Caruge, J. M.; Bawendi, M. G.; Bulovic, V. *ACS Nano* **2009**, 3 (11), 3581–3586.
- Chen, O.; Zhao, J.; Chauhan, V. P.; Cui, J.; Wong, C.; Harris, D. K.; Wei, H.; Han, H.-S.; Fukumura, D.; Jain, R. K.; Bawendi, M. G. *Nat. Mater.* **2013**, 12 (5), 445–451.
- Anikeeva, P. O.; Halpert, J. E.; Bawendi, M. G.; Bulovic, V. *Nano Lett.* **2009**, 9 (7), 2532–2536.
- Supran, G. J.; Song, K. W.; Hwang, G. W.; Correa, R. E.; Scherer, J.; Dauler, E. A.; Shirasaki, Y.; Bawendi, M. G.; Bulovic, V. *Adv. Mater.* **2015**, 27 (8), 1437–42.
- Shen, H.; Cao, W.; Shewmon, N. T.; Yang, C.; Li, L. S.; Xue, J. *Nano Lett.* **2015**, 15 (2), 1211–6.
- Dabbousi, B. O.; Bawendi, M. G.; Onitsuka, O.; Rubner, M. F. *Appl. Phys. Lett.* **1995**, 66 (11), 1316–1318.
- Mattoussi, H.; Radzilowski, L. H.; Dabbousi, B. O.; Thomas, E. L.; Bawendi, M. G.; Rubner, M. F. *J. Appl. Phys.* **1998**, 83 (12), 7965–7974.
- Schlamp, M. C.; Peng, X. G.; Alivisatos, A. P. *J. Appl. Phys.* **1997**, 82 (11), 5837–5842.
- Anikeeva, P. O.; Halpert, J. E.; Bawendi, M. G.; Bulovic, V. *Nano Lett.* **2007**, 7 (8), 2196–2200.
- Coe-Sullivan, S.; Steckel, J. S.; Woo, W. K.; Bawendi, M. G.; Bulovic, V. *Adv. Funct. Mater.* **2005**, 15 (7), 1117–1124.
- Zhao, J. L.; Bardecker, J. A.; Munro, A. M.; Liu, M. S.; Niu, Y. H.; Ding, I. K.; Luo, J. D.; Chen, B. Q.; Jen, A. K. Y.; Ginger, D. S. *Nano Lett.* **2006**, 6 (3), 463–467.
- Qian, L.; Zheng, Y.; Xue, J. G.; Holloway, P. H. *Nat. Photonics* **2011**, 5 (9), 543–548.
- Mashford, B. S.; Stevenson, M.; Popovic, Z.; Hamilton, C.; Zhou, Z.; Breen, C.; Steckel, J.; Bulovic, V.; Bawendi, M.; Coe-Sullivan, S.; Kazlas, P. T. *Nat. Photonics* **2013**, 7 (5), 407–412.
- Dai, X.; Zhang, Z.; Jin, Y.; Niu, Y.; Cao, H.; Liang, X.; Chen, L.; Wang, J.; Peng, X. *Nature* **2014**, 515 (7525), 96–99.
- Murawski, C.; Leo, K.; Gather, M. C. *Adv. Mater.* **2013**, 25 (47), 6801–6827.
- Nakanotani, H.; Higuchi, T.; Furukawa, T.; Masui, K.; Morimoto, K.; Numata, M.; Tanaka, H.; Sagara, Y.; Yasuda, T.; Adachi, C. *Nat. Commun.* **2014**, 5, 4016.
- Kim, L.; Anikeeva, P. O.; Coe-Sullivan, S. A.; Steckel, J. S.; Bawendi, M. G.; Bulovic, V. *Nano Lett.* **2008**, 8 (12), 4513–4517.
- Kim, T.-H.; Chung, D.-Y.; Ku, J.; Song, I.; Sul, S.; Kim, D.-H.; Cho, K.-S.; Choi, B. L.; Min Kim, J.; Hwang, S.; Kim, K. *Nat. Commun.* **2013**, 4, 2647.
- Cho, K.-S.; Lee, E. K.; Joo, W.-J.; Jang, E.; Kim, T.-H.; Lee, S. J.; Kwon, S.-J.; Han, J. Y.; Kim, B.-K.; Choi, B. L.; Kim, J. M. *Nat. Photonics* **2009**, 3 (6), 341–345.
- Kim, T. H.; Cho, K. S.; Lee, E. K.; Lee, S. J.; Chae, J.; Kim, J. W.; Kim, D. H.; Kwon, J. Y.; Amaralunga, G.; Lee, S. Y.; Choi, B. L.; Kuk, Y.; Kim, J. M.; Kim, K. *Nat. Photonics* **2011**, 5 (3), 176–182.
- Liu, B.; Bazan, G. C. *Conjugated Polyelectrolytes: Fundamentals and Applications*; Wiley-VCH: New York, 2012; p 438.
- Hoven, C. V.; Garcia, A.; Bazan, G. C.; Nguyen, T.-Q. *Adv. Mater.* **2008**, 20 (20), 3793–3810.
- Huang, F.; Wu, H.; Cao, Y. *Chem. Soc. Rev.* **2010**, 39 (7), 2500–2521.
- Lee, B. H.; Jung, I. H.; Woo, H. Y.; Shim, H.-K.; Kim, G.; Lee, K. *Adv. Funct. Mater.* **2014**, 24 (8), 1100–1108.
- Wu, H.; Huang, F.; Peng, J.; Cao, Y. *Org. Electron.* **2005**, 6 (3), 118–128.
- Latini, G.; Parrott, L. J.; Brovelli, S.; Frampton, M. J.; Anderson, H. L.; Cacialli, F. *Adv. Funct. Mater.* **2008**, 18 (16), 2419–2427.
- Latini, G.; Winroth, G.; Brovelli, S.; McDonnell, S. O.; Anderson, H. L.; Mativetsky, J. M.; Samori, P.; Cacialli, F. *J. Appl. Phys.* **2010**, 107 (12), 124509–124517.
- Zavelani-Rossi, M.; Lupo, M. G.; Krahne, R.; Manna, L.; Lanzani, G. *Nanoscale* **2010**, 2 (6), 931–935.
- Di Stasio, F.; Grim, J. Q.; Lesnyak, V.; Rastogi, P.; Manna, L.; Moreels, I.; Krahne, R. *Small* **2015**, 11, 1328–1334.
- Bomm, J.; Büchtemann, A.; Fiore, A.; Manna, L.; Nelson, J. H.; Hill, D.; van Sark, W. G. J. H. M. *Beilstein J. Nanotechnol.* **2010**, 1, 94–100.
- Bradshaw, L. R.; Knowles, K. E.; McDowall, S.; Gamelin, D. R. *Nano Lett.* **2015**, 15 (2), 1315–1323.
- Allione, M.; Ballester, A.; Li, H.; Comin, A.; Movilla, J. L.; Clemente, J. L.; Manna, L.; Moreels, I. *ACS Nano* **2013**, 7 (3), 2443–2452.

- (40) Rizzo, A.; Nobile, C.; Mazzeo, M.; De Giorgi, M.; Fiore, A.; Carbone, L.; Cingolani, R.; Manna, L.; Gigli, G. *ACS Nano* **2009**, *3* (6), 1506–1512.
- (41) Nam, S.; Oh, N.; Zhai, Y.; Shim, M. *ACS Nano* **2015**, *9* (1), 878–85.
- (42) Son, D. I.; Kim, H. H.; Cho, S.; Hwang, D. K.; Seo, J. W.; Choi, W. K. *Org. Electron.* **2014**, *15* (4), 886–892.
- (43) Son, D. I.; Kim, H. H.; Hwang, D. K.; Kwon, S.; Choi, W. K. *J. Mater. Chem. C* **2014**, *2* (3), 510–514.
- (44) Zhao, L.; Zhou, Z. L.; Guo, Z.; Pei, J.; Mao, S. *Development of new polymer systems and quantum dots - Polymer nanocomposites for low-cost, flexible OLED display applications. MRS Online Proc. Libr.* **2011**, *1359*, 31–42.
- (45) Bae, W. K.; Lim, J.; Zorn, M.; Kwak, J.; Park, Y.-S.; Lee, D.; Lee, S.; Char, K.; Zentel, R.; Lee, C. *J. Mater. Chem. C* **2014**, *2* (25), 4974.
- (46) Hikmet, R. A. M.; Chin, P. T. K.; Talapin, D. V.; Weller, H. *Adv. Mater.* **2005**, *17* (11), 1436–1439.
- (47) Ippen, C.; Greco, T.; Kim, Y.; Kim, J.; Oh, M. S.; Han, C. J.; Wedel, A. *Org. Electron.* **2014**, *15* (1), 126–131.
- (48) Zhang, Y.; Xie, C.; Su, H.; Liu, J.; Pickering, S.; Wang, Y.; Yu, W. W.; Wang, J.; Wang, Y.; Hahm, J.-i.; Dellas, N.; Mohney, S. E.; Xu, J. *Nano Lett.* **2011**, *11* (2), 329–332.
- (49) Rainò, G.; Stöferle, T.; Moreels, I.; Gomes, R.; Kamal, J. S.; Hens, Z.; Mahrt, R. F. *ACS Nano* **2011**, *5* (5), 4031–4036.
- (50) Christodoulou, S.; Vaccaro, G.; Pinchetti, V.; De Donato, F.; Grim, J. Q.; Casu, A.; Genovese, A.; Vicidomini, G.; Diaspro, A.; Brovelli, S.; Manna, L.; Moreels, I. *J. Mater. Chem. C* **2014**, *2* (17), 3439–3447.
- (51) Zavelani-Rossi, M.; Lupo, M. G.; Tassone, F.; Manna, L.; Lanzani, G. *Nano Lett.* **2010**, *10* (8), 3142–3150.
- (52) García-Santamaría, F.; Brovelli, S.; Viswanatha, R.; Hollingsworth, J. A.; Htoon, H.; Crooker, S. A.; Klimov, V. I. *Nano Lett.* **2011**, *11* (2), 687–693.
- (53) Xie, R.; Kolb, U.; Li, J.; Basché, T.; Mews, A. *J. Am. Chem. Soc.* **2005**, *127* (20), 7480–7488.
- (54) Sitt, A.; Salant, A.; Menagen, G.; Banin, U. *Nano Lett.* **2011**, *11* (5), 2054–2060.
- (55) Giovanella, U.; Botta, C.; Galeotti, F.; Vercelli, B.; Battiatto, S.; Pasini, M. *J. Mater. Chem. C* **2013**, *1* (34), 5322–5329.
- (56) Yap, B. K.; Xia, R.; Campoy-Quiles, M.; Stavrinou, P. N.; Bradley, D. D. C. *Nat. Mater.* **2008**, *7* (5), 376–380.
- (57) Cho, N. S.; Hwang, D.-H.; Lee, J.-I.; Jung, B.-J.; Shim, H.-K. *Macromolecules* **2002**, *35* (4), 1224–1228.
- (58) Frampton, M. L.; Sforazzini, G.; Brovelli, S.; Latini, G.; Townsend, E.; Williams, C. C.; Charas, A.; Zalewski, L.; Kaka, N. S.; Sirish, M.; Parrott, L. J.; Wilson, J. S.; Cacialli, F.; Anderson, H. L. *Adv. Funct. Mater.* **2008**, *18* (21), 3367–3376.
- (59) Brovelli, S.; Schaller, R. D.; Crooker, S. A.; García-Santamaría, F.; Chen, Y.; Viswanatha, R.; Hollingsworth, J. A.; Htoon, H.; Klimov, V. I. *Nat. Commun.* **2011**, *2*, 280.
- (60) Brovelli, S.; Bae, W. K.; Meinardi, F.; Santiago González, B.; Lorenzon, M.; Galland, C.; Klimov, V. I. *Nano Lett.* **2014**, *14* (7), 3855–3863.
- (61) Pal, B. N.; Ghosh, Y.; Brovelli, S.; Laocharoensuk, R.; Klimov, V. I.; Hollingsworth, J. A.; Htoon, H. *Nano Lett.* **2012**, *12* (1), 331–336.
- (62) Garcia-Santamaría, F.; Chen, Y. F.; Vela, J.; Schaller, R. D.; Hollingsworth, J. A.; Klimov, V. I. *Nano Lett.* **2009**, *9* (10), 3482–3488.
- (63) Meinardi, F.; Colombo, A.; Velizhanin, K. A.; Simonutti, R.; Lorenzon, M.; Beverina, L.; Viswanatha, R.; Klimov, V. I.; Brovelli, S. *Nat. Photonics* **2014**, *8*, 392–399.
- (64) Bae, W. K.; Brovelli, S.; Klimov, V. I. *MRS Bull.* **2013**, *38*, 721–30.
- (65) Bae, W. K.; Park, Y.-S.; Lim, J.; Lee, D.; Padilha, L. A.; McDaniel, H.; Robel, I.; Lee, C.; Pietryga, J. M.; Klimov, V. I. *Nat. Commun.* **2013**, *4*, 2887.
- (66) Bozyigit, D.; Yarema, O.; Wood, V. *Adv. Funct. Mater.* **2013**, *23* (24), 3024–3029.
- (67) Brovelli, S.; Bae, W. K.; Galland, C.; Giovanella, U.; Meinardi, F.; Klimov, V. I. *Nano Lett.* **2014**, *14* (2), 486–494.
- (68) Pal, B. N.; Ghosh, Y.; Brovelli, S.; Laocharoensuk, R.; Klimov, V. I.; Hollingsworth, J. A.; Htoon, H. *Nano Lett.* **2012**, *12* (1), 331–336.
- (69) Anikeeva, P. O.; Madigan, C. F.; Halpert, J. E.; Bawendi, M. G.; Bulovic, V. *Phys. Rev. B* **2008**, *78* (8), 085434.
- (70) Coe, S.; Woo, W. K.; Bawendi, M.; Bulovic, V. *Nature* **2002**, *420* (6917), 800–803.
- (71) Jing, P. T.; Zheng, J. J.; Zeng, Q. H.; Zhang, Y. L.; Liu, X. M.; Liu, X. Y.; Kong, X. G.; Zhao, J. L. *J. Appl. Phys.* **2009**, *105* (4), 044313.
- (72) Niu, Y. H.; Munro, A. M.; Cheng, Y. J.; Tian, Y. Q.; Liu, M. S.; Zhao, J. L.; Bardecker, J. A.; Jen-La Plante, I.; Ginger, D. S.; Jen, A. K. Y. *Adv. Mater.* **2007**, *19* (20), 3371–3376.
- (73) Stoudamire, J. W.; Janssen, R. A. J. *J. Mater. Chem.* **2008**, *18* (16), 1889–1894.
- (74) Zhang, Y. Q.; Cao, X. A. *Appl. Phys. Lett.* **2010**, *97* (25), 252903.
- (75) Yokoyama, D.; Sakaguchi, A.; Suzuki, M.; Adachi, C. *Appl. Phys. Lett.* **2008**, *93* (17), 173302.
- (76) Kim, S.-Y.; Jeong, W.-I.; Mayr, C.; Park, Y.-S.; Kim, K.-H.; Lee, J.-H.; Moon, C.-K.; Brüting, W.; Kim, J.-J. *Adv. Funct. Mater.* **2013**, *23* (31), 3896–3900.
- (77) Kim, J.-S.; Ho, P. K. H.; Greenham, N. C.; Friend, R. H. *J. Appl. Phys.* **2000**, *88* (2), 1073–1081.
- (78) Chi, C.; Mikhailovsky, A.; Bazan, G. C. *J. Am. Chem. Soc.* **2007**, *129* (36), 11134–11145.
- (79) Carbone, L.; Nobile, C.; De Giorgi, M.; Sala, F. D.; Morello, G.; Pompa, P.; Hytch, M.; Snoeck, E.; Fiore, A.; Franchini, I. R.; Nadasan, M.; Silvestre, A. F.; Chiodo, L.; Kudera, S.; Cingolani, R.; Krahne, R.; Manna, L. *Nano Lett.* **2007**, *7* (10), 2942–2950.